ACS OMEGA

http://pubs.acs.org/journal/acsodf

Article

Localization of the Optical Phonon Modes in Boron Nitride Nanotubes: Mixing Effect of ^{10}B Isotopes and Vacancies

Md. Sherajul Islam,* Ashraful Hossain Howlader, Rongkun Zheng, Catherine Stampfl, Jeongwon Park, and Akihiro Hashimoto

Cite This: *ACS Omega* 2022, 7, 26591−26600

Read Online

ACCESS | Metrics & More | Article Recommendations

ABSTRACT: We explored the mixing effect of ^{10}B isotopes and boron (B) or nitrogen (N) vacancies on the atomic vibrational properties of (10,0) single-wall boron nitride nanotubes (BNNTs). The forced oscillation technique was employed to evaluate the phonon modes for the entire range (0−100%) of ^{10}B isotopes and atomic vacancy densities ranging from 0 to 30%. With increasing isotope densities, we noticed a blue shift of the Raman-active A_1 phonon peak, whereas an increased density of mixed or independent B and N vacancies resulted in the emergence of a new low-frequency peak and the annihilation of the A_1 peak in the phonon density of states. High-energy optical phonons were localized as a result of both ^{10}B isotopes and the presence of mixing defects. We found an asymmetrical nature of the localization length with increasing ^{10}B isotope content, which corresponds well to the isotope-inherited localization length of carbon nanotubes and monolayer graphene. The localization length falls abruptly with the increase in concentration of both atomic vacancies (B or N) and mixing defects (^{10}B isotope and vacancies). These findings are critical for understanding heat conduction and nanoscopic vibrational investigations such as tip-enhanced Raman spectra in BNNTs, which can map local phonon energies.

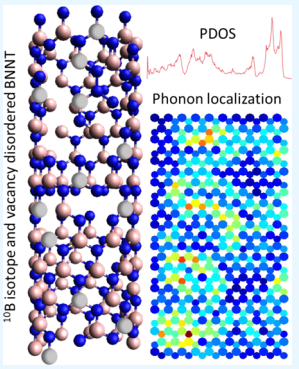

1. INTRODUCTION

Isotopes play an essential role in manipulating the physical, chemical, and biological phenomena of a material. Physical phenomena such as nuclear fission or fusion, liquid or solid magnetic resonance, and the superconducting transition temperature of metals[1,2] are due to the isotope effect. Chemical phenomena such as chemical reactions change with isotopic contents when the substituted isotopes participate directly in the chemical bonds that are broken or formed. Biological phenomena such as complex biological reactions are traced with unstable nuclei due to the isotope effect. As isotope content changes the average mass of the material, it has the most significant impact on the phonon (quanta of lattice vibrations) properties.[3] Especially in disordered nanotubes, the phonons show some peculiar transport characteristics such as ballistic, diffusive, and localized. The change in thermal conductivity in nanotubes due to the isotope effect has also been demonstrated to have a substantial impact.[4]

The isotope effects are even more pronounced in boron nitride nanotubes (BNNTs) because natural boron (B) possesses a considerable isotopic disorder. Natural BNNTs consist of 80.1% ^{11}B and 19.9% ^{10}B. Chang et al.[5] found a 50% enhancement of thermal conductivity at room temperature with 99.5% ^{11}B isotope in individual isolated multiwalled BNNTs using a microfabricated test fixture with the facility of high-resolution transmission electron microscopy. Savić et al.[6] found dominant effects on the thermal conductivity reduction with isotope disorder in BNNTs through ab initio calculations. They showed that diffusive scattering was the main source of the decrease in thermal conductivity, especially when the isotope concentration exceeded 10%. They concluded that localization effects could not be extracted from the thermal conductivity measurements. To demonstrate this dramatic increase of thermal conductivity in almost isotopically pure BNNTs, the same group developed an independent cascade scatter model of BNNTs. They modeled thermal transport in BNNTs through the atomistic Green function approach combined with first-principles phonon calculations. They revealed that isotope-induced phonon scattering inhibited phonon transport at high frequencies. In contrast, isotope enrichment enhances thermal conductivity even in a totally diffusive environment in which scatterers act independently.[7] From these studies, it is evident that the impact of isotope disruption on nanotube thermal conduction is still controversial and unclear.

On the other hand, the very first fabrication of BNNTs was described by Chopra et al.,[8] which was based on an arc

Received: May 5, 2022
Accepted: July 7, 2022
Published: July 18, 2022

discharge method. Besides the arc discharge method,[8,9] chemical vapor deposition[10,11] and laser ablation methods[12,13] are also used for synthesizing BNNTs. During these synthesis processes of BNNTs, there will be the introduction of ubiquitous atomic vacancies, similar to their two-dimensional counterpart.[14] Moreover, intentional atomic vacancy creation by irradiation was utilized to recognize the chirality of an independent wall in multiwalled BNNTs by observing the direction or the growth track of the vacancy defects.[15] Atomic vacancies alter the continuity of the regular arrangement of the hexagonal network and create dangling bonds. It has already been found that atomic vacancies may change the electrical, optical, and magnetic properties[16,17] of BNNTs. Thus, atomic vacancies should have significant effects on the phonon properties of BNNTs.

As BNNTs are structural analogues of carbon nanotubes (CNTs), it is regarded that they should show the same effects on the phonon properties due to alternation of the regular atomic arrangement, especially by isotopes and vacancies.[18,19] Moreover, phonon scattering by isotopes or vacancies significantly impact the electron−phonon interaction in BNNTs,[20] leading to the possible alteration of electron transport properties. Thus, an in-depth analysis of individual isotopes and vacancies, as well as combinations of these, in BNNTs, is indispensable. The phonon properties of pristine BNNTs have been explored in the literature using a valence shell model,[21] Ab initio calculation,[22] the force constant model,[23,24] the continuum model,[25] Raman spectroscopy,[26−29] and infrared spectroscopy.[30] Even though the phonon properties in disordered BNNTs have been discussed in several theoretical and experimental studies, a comprehensive investigation of this problem in natural systems with a large atomic scale is still absent. Moreover, to our knowledge, there is no work on phonon properties of BNNTs with both isotopes and vacancies.

Here, a systematic, detailed study of the effects of isotopes and vacancies (individual B and N atoms), as well as mixed isotopes and vacancy defects, on the phonon characteristics of BNNT is presented. The forced oscillation technique (FOT), established by Williams and Maris[31] for a disordered system with a large number of atoms, was used to determine the phonon eigenmodes of disordered BNNTs. It was found that in an isolated system having a single electron and disordered potential, the eigenmodes were in exponentially localized states, whereas the eigenmodes were in spatially diffusive states with periodic potentials. This phenomenon is called Anderson localization.[32] In a disordered system, phonons should also be confined just like electrons. In most cases, a substantial vibrational amplitude arises around defects and decays exponentially into the system's pristine area. It was perceived that the phonon modes in a disordered system shifted to the outside of the normal-frequency region.[33,34] Here, we step by step inspect the properties of vibrational modes in disordered BNNTs addressing the questions of how the modes shift and the mode patterns localize.

2. METHODS

The translation vector (T) and the chiral vector (C) of the nanotube related to its length and width, respectively, were multiplied to determine the unit cell[35] of single-walled BNNTs (SWBNNTs). Figure 1 shows the isotope and vacancy-defected ball−stick model and the Brillouin zone (BZ) of (10,0) SWBNNTs. The unit cell of a (10,0) SWBNNT consists of 20 B and 20 N atoms.

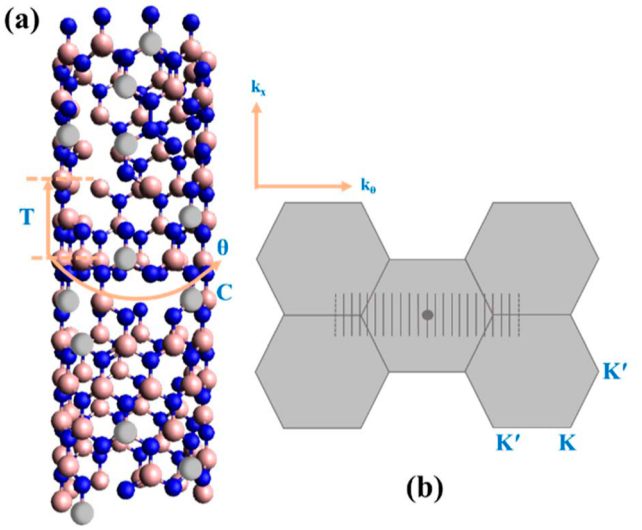

Figure 1. (a) Ball and stick model of isotope and vacancy-defected SWBNNTs. Copper-blue balls are N atoms, rosy-pink balls are ^{11}B atoms, and light-black balls are ^{10}B atoms. (b) BZ of the (10,0) zigzag SWBNNTs with high-symmetry points. The BZ consists of N number of straight lines through the k space of h-BN, each with a length of $2\pi/T$, where T and N represent the BNNT unit cell length and the number of h-BN unit cells in a single BNNT unit cell, respectively. Here, T and N are 0.435 nm and 20, respectively. k_x and k_θ are the wave vectors along the tube axis and perpendicular to it, respectively.

In this analysis, we used 125-unit cells with a total of 5000 atoms and a length of 54.37 nm. Ballistic transport of charge carriers will be possible with such a length since it is smaller than 100 nm.[36] Site percolation theory was employed to introduce ^{10}B isotope and atomic vacancies into the structure. The maximum bond probability of ∼70% can be achieved for the honeycomb site percolation structure. Thus, we investigate a wide range of vacancy densities up to 30% and isotope levels up to 100%. The fourth-nearest neighbor atomic interactions are considered using the force constants derived by Xiao et al. for the planar h-BN sheet.[37] Because of the curvature effect, the force constants of SWBNNTs and the h-BN planar sheet are not the same. We have corrected the force constants of the SWBNNT by calculating the changes in the bond angles of the cylindrical tube relative to the planar h-BN sheet. The approach to achieve the curvature effect is depicted in Figure 2a,b. Considering a force constant K, between two atoms A (B atom) and B (N atom), the projection of B on the xy-plane and its force constant tensor are denoted as B' (unfilled circle) and K', respectively, as shown in Figure 2a. K and K' rotate around the y-axis at an angle of $\phi/2$, where ϕ denotes the central angle between A and B. The projection of B' on the zx-plane and its force constant tensor are represented as B'' (unfilled circle) K'', where K'' is parallel to the x-axis. Using the new bond angles in the cylindrical SWBNNTs compared to the planar h-BN sheet, the force constants of the SWBNNTs are calculated. Table 1 shows the modified force constants.

The FOT was used to estimate the eigenstate and localization phenomena of phonons for defective SWBNNTs. Usually, a large system is required to quantify the defect effects precisely. However, the dynamical matrix technique or first-principles calculations are limited by a small-scale system.

https://doi.org/10.1021/acsomega.2c02792
ACS Omega 2022, 7, 26591−26600

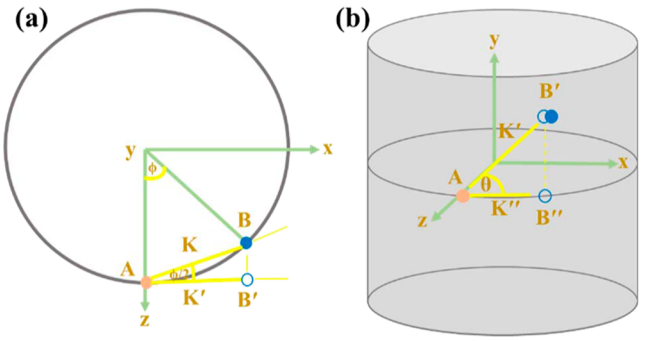

Figure 2. (a) View of SWBNNTs from the top. The projection of the B atom (filled circle) on the *xy*-plane is denoted as (unfilled circle). (b) Side view of the SWBNNT. The projection of B' (unfilled circle) on the *zx*-plane is denoted as B'' (unfilled circle).

Table 1. Corrected Force Constant Parameters for (10,0) SWBNNTs in Units of 10^4 dyn/cm by Adding the Bending Effect[a]

force constant parameters	ref.[37]	corrected force constants for (10,0) SWBNNT
$\varphi_r^{(1)}$	31.00	30.61557
$\varphi_r^{(2B-B)}$	7.00	6.737185
$\varphi_r^{(2N-N)}$	8.00	7.69964
$\varphi_r^{(3)}$	1.00	0.949699
$\varphi_r^{(4)}$	−1.90	−1.72893
$\varphi_{ti}^{(1)}$	18.50	18.27058
$\varphi_{ti}^{(2B-B)}$	−3.23	−3.10873
$\varphi_{ti}^{(2N-N)}$	−0.73	−0.702592
$\varphi_{ti}^{(3)}$	−3.25	−3.08652
$\varphi_{ti}^{(4)}$	1.29	1.17385
$\varphi_{to}^{(1)}$	5.60	5.530554
$\varphi_{to}^{(2B-B)}$	−0.70	−0.673719
$\varphi_{to}^{(2N-N)}$	−0.55	−0.52935
$\varphi_{to}^{(3)}$	0.65	0.6173044
$\varphi_{to}^{(4)}$	−0.30	−0.272988

[a]Here, r, ti, and to represent the radial, transverse in-plane, and transverse out-of-plane, respectively.

Moreover, it is also challenging to extract the low-frequency modes by these techniques. The main advantage of the FOT is that if we know only the force constants and atomic mass of the system, we can determine the phonon characteristics of any disordered, complex, and large system over the whole frequency range by calculating the total energy of the system without knowing the phonon lifetime.

The principal idea of the FOT comes from the resonance of a mechanical system upon application of excitation. A resonant state with frequency Ω can be acquired in a lattice dynamical system if an uninterrupted excitation having an exterior continuous periodic force of frequency Ω is imparted to the system for a long time. If M_l and u_l, respectively, are the mass and displacement of the lth atom of a lattice dynamical system consisting of N atoms, the equation of motion of the system can be described as

$$M_l\ddot{u}_l(t) + \sum_{l'} \varphi_{ll'}u_{l'}(t) = F_l\cos(\Omega t) \tag{1}$$

where the spring constant among the lth atom and l'th atom is $\varphi_{ll'}$ and F_l is the continuous periodic exterior force. The mathematical expression of F_l is $F_l = F_0\sqrt{M_l}\cos(\phi_l)$. Here, F_0 is a time-independent constant and ϕ_l is an arbitrary number between 0 to 2π. We can write the displacement u_l of the system as

$$u_l(t) = \sum_{\lambda} Q_\lambda(t)\frac{e_l(\lambda)}{\sqrt{M_l}} \tag{2}$$

where Q_λ corresponds to a normal mode and Q_λ (t) and e_l (λ) are the magnitude and displacement values of λ, respectively. The average value of E can be obtained by averaging all possible ϕ_l values as

$$\langle E\rangle = \frac{F_0^2}{4}\sum_{\lambda}\frac{\sin^2\{[(\omega_\lambda - \Omega)/2]t\}}{(\omega_\lambda - \Omega)^2} \tag{3}$$

The modes whose frequencies fall within the range about $\mp(2\pi/t)$ of Ω contribute to the sum in eq 3. t is chosen in such a way that $\Omega t \gg 1$, which means that the sum in eq 3 is contributed by only a small range of frequency modes in the Ω scale. The number of such modes are greater than unity. Thus, the sum in eq 3 can be represented as a delta (δ) function, which provides the average energy as

$$\langle E\rangle \approx \frac{\pi t F_0^2}{8}\sum_{\lambda}\delta(\omega_\lambda - \Omega) = \frac{\pi t F_0^2 N g(\Omega)}{8} \tag{4}$$

where $g(\Omega)$ signifies the partial density of states (PDOS). Hence, the task is reduced to obtaining the time evolution of the equations of motion upon application of an external force. If time t is discretized with a step τ, the equations of motion can be expressed as

$$v_l(n+1) = v_l(n) + M_l^{-1}\left[\sum_{l'}\varphi_{ll'}u_{l'}(n) + F_l\cos(\Omega n\tau)\right]\tau \tag{5}$$

$$u_l(n+1) = u_l(n) + v_l(n)\tau \tag{6}$$

where n is the number of time steps defined as $t = n\tau$. The step size τ should be small enough to get a fine resolution. Here, τ is chosen as 0.01×10^{-13}. Usually, typical atomic vibrational frequencies lie within the range of approximately 10^{12} to 10^{14} Hz. Thus, the frequency of the external applied force is chosen as 10^{13} Hz to extract each frequency mode of the system. The system reaches the resonant condition after a long period of external excitation. Under the resonant condition, the average total energy of the system is calculated from which the PDOS is calculated as

$$g(\Omega) = \frac{8\langle E\rangle}{\pi t F_0^2 N} \tag{7}$$

The eigenvector of the disordered SWBNNT is also calculated. After driving the system for a certain reasonable time period T, $u_l^{(1)}$ becomes the new displacement of an atom l. Following that time period, a new force with a new value is assigned to atom l and is written as $F_l^{(1)} = u_l^{(1)}M_l$. The eventual displacement after p iterations can be represented as

$$u_l^{(p)} \approx \frac{Ce_l(\lambda_1)}{\sqrt{M_l}} \tag{8}$$

here, C stands for a constant. Therefore, the spatial eigenvector for the mode λ_1 can be attained.

https://doi.org/10.1021/acsomega.2c02792
ACS Omega 2022, 7, 26591−26600

3. RESULTS AND DISCUSSION

Figure 3 shows the estimated PDOS of ^{10}B isotope-containing (0−100%) SWBNNTs. As expected, Van Hove singularities

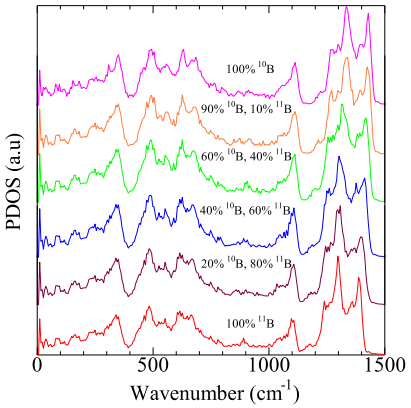

Figure 3. PDOS of BNNTs with various ^{10}B and ^{11}B isotope concentrations.

appear in the estimated PDOS caused by the confinement effect of the reduced dimensionality of SWBNNTs. The PDOS successfully generates all the distinctive peaks associated with the sp^2 bonded B−N compound. The estimated PDOS is quite similar to that of the 2D h-BN sheet, except for tiny peaks induced by one-dimensional singularities. The high-energy in-plane tangential G-band phonon modes [longitudinal optical (iLO) and transverse optical (iTO)] are of primary attention in this study. Generally, the E_{2g} peak in PDOS is Raman-active in armchair-edged BNNTs, similar to 2D h-BN; however, the A_1 peak is Raman-active in zigzag-edged BNNTs.[21,22,24,27,29] We observe the A_1 peak at 1376 cm^{-1} in our simulations to be smaller than the value (E_{2g}) obtained for 2D h-BN[38] due to the curvature effect.[18] The curvature effect of BNNTs softens this Raman-active mode frequency to the lower value, which is consistent with the earlier results.[39]

A general trend of moving all vibrational modes toward the higher-energy region is found when the ^{10}B isotope level increases. The A_1 peak has a considerable upward shift due to the isotope interaction. The previous studies found that adding a lighter (heavier) isotope atom generates a large upward or downward move in the high-frequency phonon mode.[40,41] However, the effect was negligible in the low-frequency regime.[19,39] Usually, the phonon lifetime for the low-frequency phonon modes for carbon-based and similar BN structures shows power law behavior. Moreover, in-plane and out-of-plane phonon modes have vastly different lifetime scales because of their vastly different stiffness. Consequently, isotope impurities affect the high-frequency phonon modes sensitively but not the low-frequency modes for these types of structures. Prior studies also revealed that the incorporation of heavier isotope atoms causes a significant downward shift of the high-frequency phonon mode, whereas the impact is weaker in the low-frequency regime.[42,43] Isotopic substitution decreases the average atomic mass of BNNTs, and even a minor amount of isotope in BNNTs can drastically alter the phonon characteristics. An upward shift of the Raman-active phonon modes was also detected in ^{10}B isotope-containing BNNTs in the earlier study.[44] The frequency of vibrational mode ω is related to the atomic mass M as $\omega \propto M^{-1/2}$, showing that lowering the mass can raise the frequency.

Using the standard harmonic oscillator theory, the linear upward shift of frequencies due to isotope defects can be described as

$$\omega_{10_B}(x) = \frac{\omega_{11_B}}{\sqrt{1 - \frac{x}{11}}} \quad (9)$$

Here, ω_{11_B} and x signify the frequency of original BNNTs and the ^{10}B isotope contents, respectively. The upward shift of the A_1 peak as a function of ^{10}B isotope concentration is depicted in Figure 4. A comparison of the values obtained from eq 9

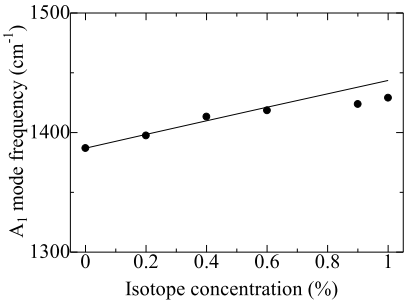

Figure 4. ^{10}B isotope concentration vs Raman-active A_1 mode frequency. The solid line is extracted from the simple harmonic oscillator model described in eq 9.

with the results of our computation is also shown. The solid line represents the computed values of the prior relation, whereas circles reflect our computational results. We discover that our computational results and theoretical values are perfectly consistent. From 0 to 100% ^{10}B isotope contents, the A_1 mode shifts upward by about 42 cm^{-1}. The system contains the same mass for both 0 and 100% ^{10}B isotope concentrations. However, the harmonic arrangement is disrupted beyond these two extreme situations, and the mass of the nanotube should be the inverse of the square root of both ^{11}B and ^{10}B atoms. With the increase of ^{10}B atoms in the system, the average atomic mass decreases, resulting in a phonon frequency shift to the high-energy regime.

Next, we concentrate our investigation on the impacts of vacancies on BNNT phonon behavior. Vacancy defects have been demonstrated to induce considerable deviations in phonon and heat conduction characteristics of CNTs in previous studies. The bond length and energy can be altered by vacancies, and the vibrational frequency is highly reliant on these parameters.[45] Because of significant changes in the phonon structure,[46−48] the effect of vacancy defects on thermal conductivity is more noticeable than that of isotopes. An earlier study[49] showed that the thermal conductivity of a graphene nanoribbon (GNR) was reduced by 81% even at a relatively low concentration of vacancies (0.1%). Different studies on CNTs[50−52] manifested that 1−2% vacancy concentration resulted in about a 50% reduction in the thermal conductivity.

Again, some studies on silicene nanoribbons[53] and silicon nanotubes[54] found around a 50% reduction in thermal conductivity with 1−2% atomic vacancy concentration. Thus, the effects of vacancies on the phonon characteristics of BNNTs are exciting. The impact of various concentrations of B and N vacancies on the PDOS of BNNTs is presented in Figure 5a,b. Although the ^{10}B isotope disorder causes an upward swing in vibrational frequencies, the PDOS peaks show

https://doi.org/10.1021/acsomega.2c02792
ACS Omega 2022, 7, 26591−26600

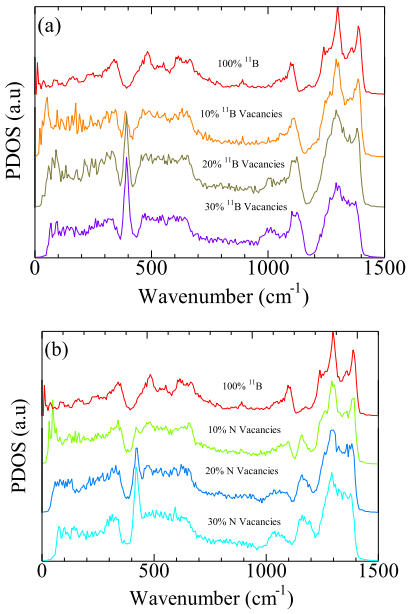

Figure 5. PDOS values of SWBNNTs with (a) ^{11}B vacancies and (b) N vacancies.

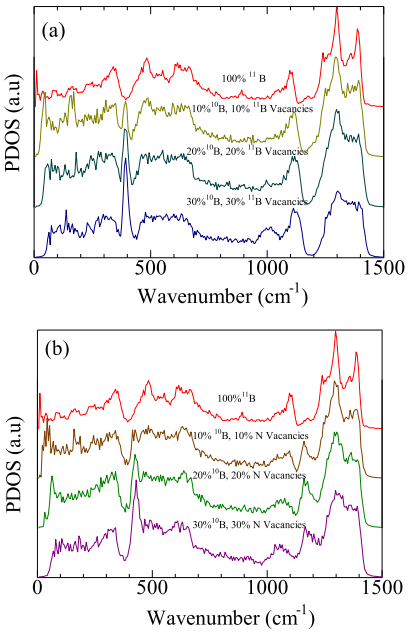

Figure 6. PDOS values of BNNTs with a (a) mixture of ^{10}B isotope and B vacancies and a (b) mixture of ^{10}B isotope and N vacancies.

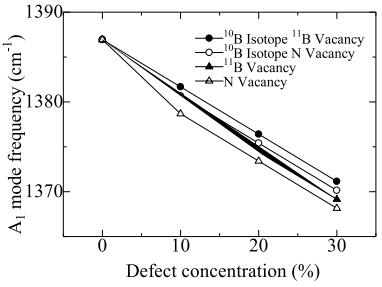

Figure 7. Impurity concentration vs A_1 mode frequency.

a widening and downward shift as the vacancy concentration rises. For both types of vacancies, the A_1 peak has totally vanished at 10% and higher densities. Using the bond-order theory, Xie et al.[55] demonstrated that phonons in 2D materials are dispersed greatly by atomic vacancies. Vacancy disorders can also change the periodicity of the sp^2-hybridized BNNT structure. The momentum conservation of the crystal is broken due to the disruption of the periodic order by the significant density of vacancies. Consequently, the high-energy phonon peaks no longer appear.

The emergence of several abrupt peaks at low frequency with increasing vacancy concentration is another key feature of the phonon mode, as seen in Figure 5. The concentrations of unsaturated bonds of B and N atoms increase with increasing vacancy concentration, which may cause a decrease in the high-frequency phonon density. As a result, phonon modes migrate toward the low-energy region. Phonon scattering in the low-frequency region due to the defects was notable in CNTs, as demonstrated by Mingo et al.[56] In addition to generating a substantial peak, increasing defect density also lowers the average PDOS in the low-frequency zone. Mahan et al.[57] discovered the low-frequency flexural phonon modes with a quadratic dispersion in the PDOS of CNTs. On the other hand, Mariani et al.[58] and Ochoa et al.[59] showed that the average PDOS of graphene reduces due to the stiffening of the flexural phonon modes caused by the disorder-induced strain. Jeon et al.[24] found flexure phonon modes in BNNTs even though the constituting atoms (B and N) are polar in nature. We believe that vacancies stiffen the flexural phonons, resulting in a drop in the average PDOS in the low-frequency region.

The effect of isotope mixing with B or N vacancies on the BNNT PDOS is depicted in Figure 6. Although the isotope disorder causes an upward change in phonon modes, the combination of the isotope and vacancies appears to have a downward shift. The vacancy disorder in BNNTs, however, induces a more significant downward shift than the mixing defects. As shown in Figure 7, the softening of the A_1 peak is highly influenced by defect density, with the descending shift being greater for B vacancies than for other defects. Simon et al.[60] also found similar results. They created a double-walled CNT in which the inner wall was ^{13}C enriched and the exterior wall was natural carbon (i.e., 1.1% ^{13}C and 98.9% ^{12}C) enriched along with inevitable vacancies. The ^{13}C-enhanced inner wall of the CNT caused a nonuniform expansion and descending shift of the tangential G mode. The inevitable point defects present in a system have a considerable impact on the phonon scattering owing to the extreme sensitivity of phonon to mass disorder. The scattering generated by point defects may cause the phonon to traverse through new states, causing the PDOS to broaden. Furthermore, in a system having a breakdown in its lattice symmetry by defects, the atomic vibrations in that system can be identified outside of the ideal system's normal frequency range.[33,34] In a defect-free environment, phonons are unrestricted to move; however, in the presence of isotopes or vacancies, phonons become confined. In disordered systems, the phonon mean free path changes according to the square of the localization length. As a result, the phonon energy may collect at its defective area, similar to the Anderson localization of electrons.[32] The static localized phonons lose their heat-carrying properties. As a result, the standard transmission of thermal energy through the sample material is hampered by these localized phonons. However, phonon localization in low- dimensional materials can be beneficial in a variety of applications, including thermoelectric

https://doi.org/10.1021/acsomega.2c02792
ACS Omega 2022, 7, 26591−26600

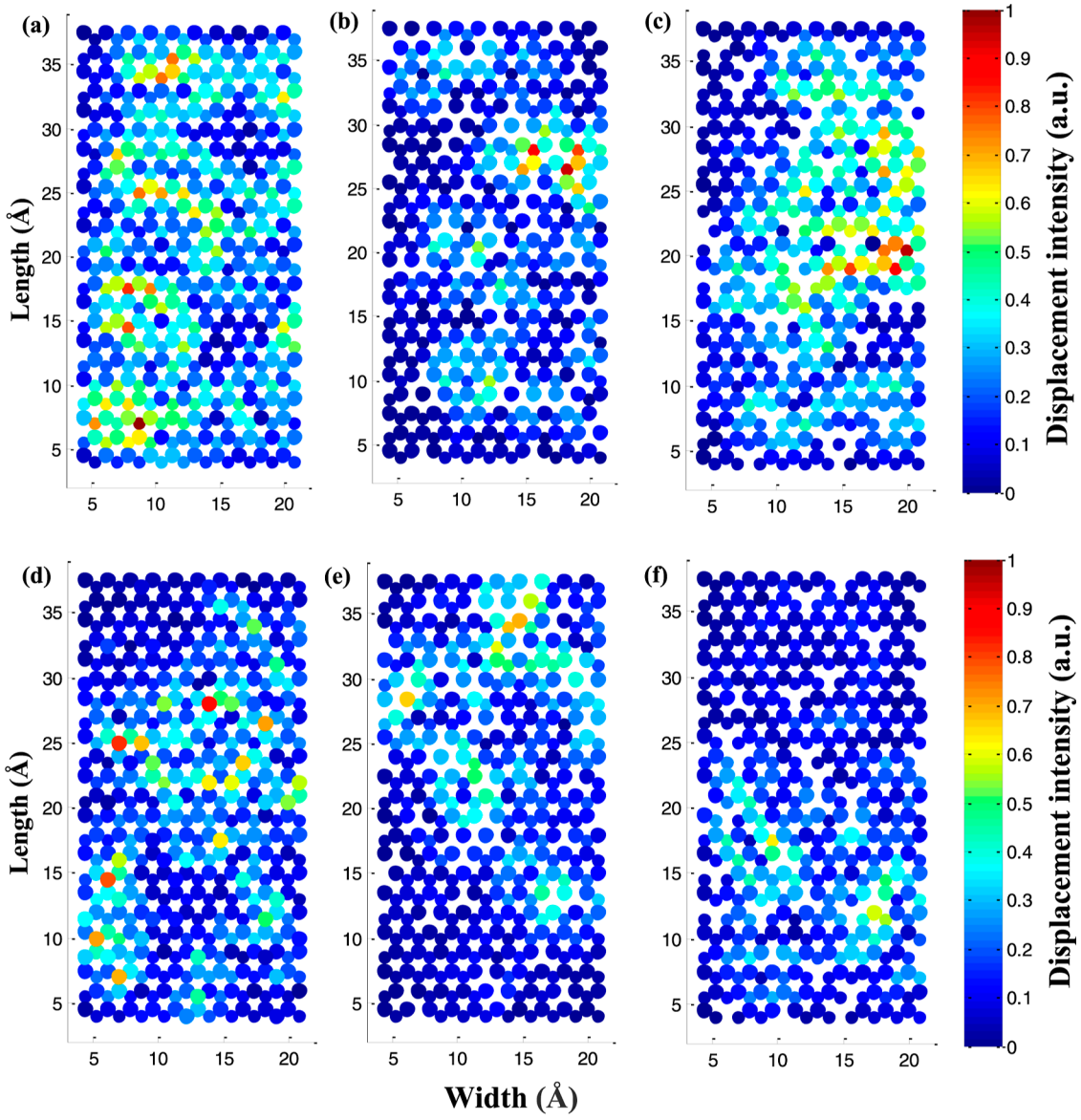

Figure 8. Typical mode patterns at ω = 1376 cm^{-1} for unfolded SWBNNTs with (a) pristine, (b) 20% B vacancy, (c) 20% N vacancy, (d) 20% ^{10}B isotope, 20% combined (e) 10% ^{10}B isotope and 10% B vacancies, and (f) 10% ^{10}B isotope and 10% N vacancy-defected structures. Each circle denotes an atom (smaller circles are ^{10}B atoms and larger circles are ^{11}B atoms), and the colors denote the displacement, which is linearly normalized by the maximum value. The intensity of the displacement of each atom is presented by the color bar.

energy conversion and microelectronic heat management.[61−63] The normal linewidth of the Raman spectra is also caused by localized phonons.[27] To explain the experimental findings, a better understanding of isotope phonon localization and vacancy-induced BNNTs is required.

The atomic-scale localization behavior of phonon modes in SWBNNTs has also been investigated in the presence of isotope and vacancy defects. In a perfect system, the wave of a phonon is disturbed. However, phonons can go through ballistic, diffusive, or confined regions in a disordered structure. Defects cause the disruption of the momentum conservation of the system. As a result of the interruption of momentum conservation of the regular atomic arrangement, the wave vectors of phonons cannot occupy regular quantum numbers. The phonons disperse into various phonon states and become spatially confined. There have been numerous attempts to estimate and display the phonon localization events in isotope-defected nanostructures. Savić et al.[6] performed a first-principles analysis to investigate phonon transmission in ^{14}C isotope-enriched CNTs and ^{10}B isotope-disordered BNNTs, claiming that the thermal conductivity decrease in isotope-disordered CNTs and BNNTs is due to diffusive scattering, whereas localization of phonons was not considered. Because heat transport happens with ballistic and diffusive phonons, they reasoned that phonon localization could not be seen. They projected that localization effects would arise in optical modes with short wavelengths. As a result, to see any localization effects, separate experimental techniques competent for exploring these high-energy modes are necessary. Using molecular dynamics modeling, Li et al.[64] examined the heat transport of isotope-disordered GNRs and CNTs. They discovered that the loss in thermal conductivity in CNTs is more significant than in GNR owing to strong optical phonon localization. They calculated the phonon dispersion relation in an attempt to depict the localized phonon modes but were unable to obtain the actual image of the localization effect. The

https://doi.org/10.1021/acsomega.2c02792
ACS Omega 2022, 7, 26591−26600

mixing effect of ^{10}B isotopes and vacancies, as well as their independent effect on the phonon localization in unfolded SWBNNTs, has been explored here. We are particularly interested in high-frequency tangential phonon modes.

Figure 8 depicts the atomic vibrational patterns for the A_1 phonon mode at 1376 cm^{-1}. The vibrational patterns displayed here are based on 460 sites only. A sufficiently localized mode can be retained in this site area, which reduces the need for a significant number of atoms. The circle in Figure 8 specifies an atom; larger circles denote ^{11}B atoms, smaller circles indicate ^{10}B atoms, and different hues represent the strength of the displacement. The mode pattern for pure BNNTs is shown in Figure 8a.

The modes present an unequal distribution across the entire sample area. The mode patterns are determined by imposing a random force proportionate to the displacement of atoms at each time step iteratively. As a result, the eigenmode positions are expected to change over time. The randomness of the eigenmodes could be due to other factors. Usually, optical phonons experience more frequent scattering due to their high density compared to the acoustic phonon in the PDOS. The range of possible scattering outcomes is increased since scattering activities are generally inelastic.[65] Consequently, the coherent backscattering strength decreases owing to the reduced possibility of a specific mode reversing its scattering order. However, to achieve a high coherent backscattering effect, scattering events should be entirely elastic.[66] As a result, eigenmodes in the sample may appear at random.

The presence of the ^{10}B isotope or vacancies in the SWBNNT structure induces a spatially localized eigenmode in the displacement pattern. Figure 8b–d shows the mode patterns with a 20% randomly oriented ^{10}B isotope and B or N vacancy-defected sample. Few modes are observed to be confined and scattered irregularly across the sample area. The displacement pattern for isotope (10%) mixing with vacancies (10%) is shown in Figure 8e,f. The vibrational modes are not adequately diffused in this example, and some vibrational modes are severely confined. Only a few atoms vibrating with the highest amplitude are discovered concentrated near the vacancy defects, indicating a significant localization. The location of localized atoms remains unevenly distributed near the vacancies, and it evolves through time. With increasing defect concentrations, the localization impact becomes more substantial. Prior investigation revealed that the thermal conductivity of nanotube structures reduces with cumulative defect concentrations. The localization of phonons due to the defects provides important evidence for earlier findings because phonons are the primary heat carrier in semiconducting nanostructures.

To further illustrate the degree of localization, the inverse participation ratio (IPR) of the system is derived. It is possible to express the IPR in the following way

$$\mathrm{IPR} = \frac{\sum_{l=1}^{N} |u_{l,\lambda}|^4}{\left(\sum_{l=1}^{N} |u_{l,\lambda}|^2\right)^2} \tag{10}$$

where $u_{l,\lambda}$ represents the eigenmode's displacement of the lth atom. In the localized state, a limited number of atoms oscillate with the largest displacement. Considering the normalization of the eigenvector among the n number of atoms, the amplitude the localized atom is $u = 1/\sqrt{n}$. IPR = $1/n$ can now be used to represent the inverse participation ratio. It is worth noting that the strong localization can be achieved when n = 1 (i.e., IPR = 1), and only one atom oscillates in that mode. With $n = N$ and IPR = $1/N$, a dispersed oscillation pattern with all atoms vibrating at the same amplitude of $u = 1/\sqrt{N}$ should be noticed. We calculated the localization length L_λ from the value of IPR, which is correlated with the IPR as $L_\lambda \propto \mathrm{IPR}^{-1/2}$,[67] and the L_λ of the state λ can be described as

$$\frac{L_\lambda}{L_0} = \left(\frac{\mathrm{IPR}_0}{\mathrm{IPR}_\lambda}\right)^{1/2} \tag{11}$$

where L_0 is the unfolded SWBNNT size, that is, the 2D h-BN sheet, and IPR_0 is the average value of IPR_λ.

Figure 9 shows the fluctuation of L_λ with the variation of isotope concentration. The simulation was run with 5000 atoms at = 1376 cm^{-1} for the A_1 mode phonon. The filled circles in Figure 9 denote the average of 10 eigenmodes. L_λ is associated with IPR_λ as $L_\lambda \infty \mathrm{IPR}_\lambda^{-1/2}$. It is projected that strong localization will be obtained with the shortest localization length and vice versa. According to the calculations, the localization length decreases dramatically when isotope contents elevate from 0 to 60% and then rise again from 60 to 100%. At a 60% isotope content, the minimum localization length was discovered.

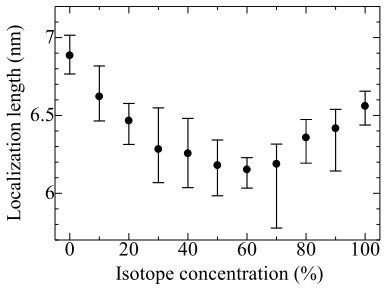

Figure 9. Localization length as a function of ^{10}B isotope concentration.

Despite the asymmetrical behavior, this finding is consistent with the earlier work on single-layer graphene by Rodriguez-Nieva et al.[43] A variety of reasons could cause this erratic character. The influence of decreasing the mass of a system (by adding ^{10}B isotopes to a ^{11}B lattice) differs from that of increasing the system's mass (by adding ^{11}B isotopes to a ^{10}B lattice). L_λ is calculated from the IPR, which is derived from the eigenstate amplitudes of atoms. The total mass of the system decreases as ^{10}B atoms are added to the ^{11}B lattice. This eigenstate amplitude of the atoms with reduced mass will be larger than the pristine structures' eigenstate amplitude. The same thing happens when ^{11}B impurities are introduced into a ^{10}B lattice. In both circumstances, the eigenstates of the pristine structure are smaller than the IPR, causing a lower L_λ. In the reduced mass case, the effect of isotope addition is stimulatingly abrupt. As a result, the localization length may have an asymmetrical characteristic. There could be additional explanations for the asymmetry.

The localization of phonons in the flat zones of dispersion relation can readily happen as described by Savić et al.[6] Besides, they[6] also revealed that optical phonons in the high-frequency region are predominantly localized.[6] The defect-related backscattering is considerable in the optical phonons in the high-frequency region, as observed in CNTs.[68] An island with a different frequency is developed for the localized

https://doi.org/10.1021/acsomega.2c02792
ACS Omega 2022, 7, 26591−26600

eigenstate compared to the rest of the atoms, which may be the physical origin of localization.

The L_λ value for different combinations of defects has also been extracted, as shown in Figure 10. The values of L_λ decay noticeably with the rise of mixing defects or separate B or N point vacancies, as shown in Figure 10. For the same defect density, the combined defects demonstrate a sudden decrease in behavior in comparison to isotope disorder. This is because the bond length and energy change when vacancies form in the lattice structure, which modifies the force constant parameters. The force constants for the ^{10}B isotope-containing sample, on the other hand, stay unchanged since the bonding chemistry is unaffected by the additional neutron in each nucleus. However, because of the mass change of the ion, the isotope defect affects the dynamics. Because the frequency f is related to the system mass m as the inverse of the square root (i.e., $f \propto m^{-1/2}$), changes in ^{10}B isotope mass can significantly modify the PDOS. The isotope mixing with vacancies, however, changes the PDOS more suddenly. Thus, the comparison of the L_λ for different impurity concentrations and different types of defects is not straightforward. As a result, there may be a sharp drop in L_λ.

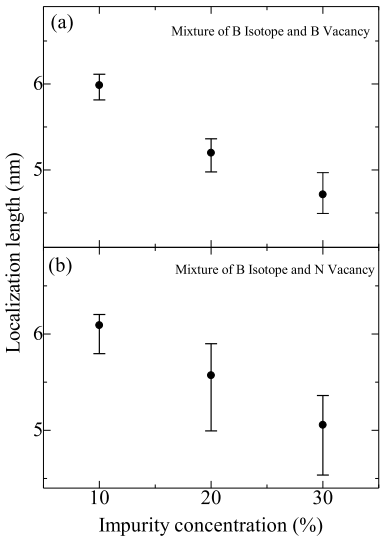

Figure 10. Impurity concentration vs localization length of BNNTs with a mixture of ^{10}B isotope and (a) B and (b) N vacancies.

4. CONCLUSIONS

In summary, the FOT was used to investigate the effects of ^{10}B isotope mixing with B or N point vacancies on SWBNNT phonon modes. The PDOS analysis revealed that the Raman-active A_1 phonon peak is highly prone to both ^{10}B isotope and vacancy disorders. With increasing isotope levels, the A_1 mode exhibited a fairly linear downshift to the low-frequency region. A stronger downshift in the A_1 mode was observed for vacancy defects than for the isotope, and it vanished when defect concentrations reached a certain level. In the low-energy regime, the mixing defects generated a new sharp peak. We created typical mode patterns for different types of disordered structures to demonstrate the phonon localization processes caused by the defects. Both ^{10}B isotope and mixing defects caused high-energy optical phonons to be localized. With increasing ^{10}B isotope levels, we discovered an asymmetrical character of the localization length, which corresponds well to the isotope-inherited localization length of CNTs and monolayer graphene. With the inclusion of separate B or N point vacancies as well as mixing defects, the localization length reduced abruptly. This paper gives a theoretical framework for isotope- and vacancy-induced phonon properties, which is crucial for understanding SWBNNT thermal conductivity and Raman spectra.

AUTHOR INFORMATION

Corresponding Author

Md. Sherajul Islam − *Department of Electrical and Electronic Engineering, Khulna University of Engineering and Technology, Khulna 9203, Bangladesh; Department of Electrical and Biomedical Engineering, University of Nevada, Reno, Nevada 89557, United States;* orcid.org/0000-0002-6717-2523; Phone: +17754629960; Email: sheraj_kuet@eee.kuet.ac.bd

Authors

Ashraful Hossain Howlader − *School of Physics, The University of Sydney, Sydney, New South Wales 2006, Australia;* orcid.org/0000-0002-7227-9077

Rongkun Zheng − *School of Physics, The University of Sydney, Sydney, New South Wales 2006, Australia;* orcid.org/0000-0002-7860-2023

Catherine Stampfl − *School of Physics, The University of Sydney, Sydney, New South Wales 2006, Australia*

Jeongwon Park − *School of Electrical Engineering and Computer Science, University of Ottawa, Ottawa ON K1N 6N5, Canada; Department of Electrical and Biomedical Engineering, University of Nevada, Reno, Nevada 89557, United States*

Akihiro Hashimoto − *Graduate School of Engineering, University of Fukui, Fukui 910-8507, Japan*

Complete contact information is available at: https://pubs.acs.org/10.1021/acsomega.2c02792

Author Contributions

M.S.I. conceived the work; M.S.I. and A.H.H. performed the simulations and wrote the manuscript under the supervision of J.P. and A.H.; R.Z. and C.S. interpreted the data; all authors discussed and analyzed the data and contributed during the writing of the manuscript.

Notes

The authors declare no competing financial interest.

The data that support the findings of this study are available from the corresponding author upon reasonable request.

ACKNOWLEDGMENTS

This work was partially funded by the NV NASA EPSCoR RID Seed Grant (grant number 80NSSC19M0056).

REFERENCES

(1) Reynolds, C. A.; Serin, B.; Wright, W. H.; Nesbitt, L. B. Superconductivity of Isotopes of Mercury. *Phys. Rev.* **1950**, *78*, 487.

(2) Maxwell, E. Isotope Effect in the Superconductivity of Mercury. *Phys. Rev.* **1950**, *78*, 477.

(3) Plekhanov, V. Effects Related to Isotopic Disorder in Solids. *Isotopes in Condensed Matter*; Plekhanov, V., Ed.; Springer: Berlin, Heidelberg, 2013; pp 151−206.

(4) Maruyama, S.; Igarashi, Y.; Taniguchi, Y.; Shiomi, J. Anisotropic Heat Transfer of Single-Walled Carbon Nanotubes. *J. Therm. Sci. Technol.* **2006**, *1*, 138−148.

https://doi.org/10.1021/acsomega.2c02792
ACS Omega 2022, 7, 26591−26600

(5) Chang, C. W.; Fennimore, A. M.; Afanasiev, A.; Okawa, D.; Ikuno, T.; Garcia, H.; Li, D.; Majumdar, A.; Zettl, A. Isotope Effect on the Thermal Conductivity of Boron Nitride Nanotubes. *Phys. Rev. Lett.* **2006**, *97*, 085901.
(6) Savić, I.; Mingo, N.; Stewart, D. A. Phonon Transport in Isotope-Disordered Carbon and Boron-Nitride Nanotubes: Is Localization Observable? *Phys. Rev. Lett.* **2008**, *101*, 165502.
(7) Stewart, D. A.; Savić, I.; Mingo, N. First-Principles Calculation of the Isotope Effect on Boron Nitride Nanotube Thermal Conductivity. *Nano Lett.* **2009**, *9*, 81−84.
(8) Chopra, N. G.; Luyken, R. J.; Cherrey, K.; Crespi, V. H.; Cohen, M. L.; Louie, S. G.; Zettl, A. Boron Nitride Nanotubes. *Science* **1995**, *269*, 966−967.
(9) Loiseau, A.; Willaime, F.; Demoncy, N.; Hug, G.; Pascard, H. Boron Nitride Nanotubes with Reduced Numbers of Layers Synthesized by Arc Discharge. *Phys. Rev. Lett.* **1996**, *76*, 4737−4740.
(10) Özmen, D.; Sezgi, N. A.; Balcı, S. Synthesis of Boron Nitride Nanotubes from Ammonia and a Powder Mixture of Boron and Iron Oxide. *Chem. Eng. J.* **2013**, *219*, 28−36.
(11) Zhong, B.; Huang, X.; Wen, G.; Yu, H.; Zhang, X.; Zhang, T.; Bai, H. Large-Scale Fabrication of Boron Nitride Nanotubes via a Facile Chemical Vapor Reaction Route and Their Cathodoluminescence Properties. *Nanoscale Res. Lett.* **2011**, *6*, 1−8.
(12) Golberg, D.; Bando, Y.; Eremets, M.; Takemura, K.; Kurashima, K.; Yusa, H. Nanotubes in Boron Nitride Laser Heated at High Pressure. *Appl. Phys. Lett.* **1996**, *69*, 2045−2047.
(13) Arenal, R.; Stephan, O.; Cochon, J.-L.; Loiseau, A. Root-Growth Mechanism for Single-Walled Boron Nitride Nanotubes in Laser Vaporization Technique. *J. Am. Chem. Soc.* **2007**, *129*, 16183−16189.
(14) Jin, C.; Lin, F.; Suenaga, K.; Iijima, S. Fabrication of a Freestanding Boron Nitride Single Layer and Its Defect Assignments. *Phys. Rev. Lett.* **2009**, *102*, 195505.
(15) Cheng, G.; Yao, S.; Sang, X.; Hao, B.; Zhang, D.; Yap, Y. K.; Zhu, Y. Evolution of Irradiation-Induced Vacancy Defects in Boron Nitride Nanotubes. *Small* **2016**, *12*, 818−824.
(16) Okada, S. Atomic Configurations and Energetics of Vacancies in Hexagonal Boron Nitride: First-Principles Total-Energy Calculations. *Phys. Rev. B: Condens. Matter Mater. Phys.* **2009**, *80*, 161404.
(17) Pierret, A.; Nong, H. Role of structural defects in the ultraviolet luminescence of multiwall boron nitride nanotubes. *J. Appl. Phys.* **2015**, *118*, 234307.
(18) Howlader, A. H.; Islam, M. S.; Tanaka, S.; Makino, T.; Hashimoto, A. Vacancy and Curvature Effects on the Phonon Properties of Single Wall Carbon Nanotube. *Jpn. J. Appl. Phys.* **2018**, *57*, 02CB08.
(19) Islam, Md. S.; Howlader, A. H.; Anindya, K. N.; Zheng, R.; Park, J.; Hashimoto, A. Phonon Localization in Single Wall Carbon Nanotube: Combined Effect of 13C Isotope and Vacancies. *J. Appl. Phys.* **2020**, *128*, 045108.
(20) Vokhmintsev, A.; Weinstein, I.; Zamyatin, D. Electron-Phonon Interactions in Subband Excited Photoluminescence of Hexagonal Boron Nitride. *J. Lumin.* **2019**, *208*, 363−370.
(21) Popov, V. N. Lattice Dynamics of Single-Walled Boron Nitride Nanotubes. *Phys. Rev. B: Condens. Matter Mater. Phys.* **2003**, *67*, 085408.
(22) Vibrational properties of boron-nitride nanotubes: effects of finite length and bundling|IEEE Journals & Magazine|IEEE Xplore. 2003.
(23) Saxena, P.; Sanyal, S. P. Phonon Structure and Dynamics of Boron Nitride Single Wall Nanotube. *Phys. E* **2004**, *24*, 244−248.
(24) Jeon, G. S.; Mahan, G. D. Lattice Vibrations of a Single-Wall Boron Nitride Nanotube. *Phys. Rev. B: Condens. Matter Mater. Phys.* **2009**, *79*, 085424.
(25) Pérez-Álvarez, R.; Santiago-Pérez, D. G.; Chico, L. Continuum Model for Low-Frequency Phonons of Boron Nitride Nanotubes. *Phys. E* **2015**, *74*, 129−134.
(26) Zhi, C.; Bando, Y.; Tang, C.; Golberg, D.; Xie, R.; Sekigushi, T. Phonon Characteristics and Cathodolumininescence of Boron Nitride Nanotubes. *Appl. Phys. Lett.* **2005**, *86*, 213110.
(27) Arenal, R.; Ferrari, A. C.; Reich, S.; Wirtz, L.; Mevellec, J.-Y.; Lefrant, S.; Rubio, A.; Loiseau, A. Raman Spectroscopy of Single-Wall Boron Nitride Nanotubes. *Nano Lett.* **2006**, *6*, 1812−1816.
(28) Fakrach, B.; Rahmani, A.; Chadli, H.; Sbai, K.; Sauvajol, J.-L. Raman Spectrum of Single-Walled Boron Nitride Nanotube. *Phys. E* **2009**, *41*, 1800−1805.
(29) Aydin, M. Vibrational and Electronic Properties of Single-Walled and Double-Walled Boron Nitride Nanotubes. *Vib. Spectrosc.* **2013**, *66*, 30−42.
(30) Near-Field Infrared Pump−Probe Imaging of Surface Phonon Coupling in Boron Nitride Nanotubes |The Journal of Physical Chemistry Letters. 2016.
(31) Williams, M. L.; Maris, H. J. Numerical Study of Phonon Localization in Disordered Systems. *Phys. Rev. B: Condens. Matter Mater. Phys.* **1985**, *31*, 4508−4515.
(32) Anderson, P. W. Absence of Diffusion in Certain Random Lattices. *Phys. Rev.* **1958**, *109*, 1492−1505.
(33) Maradudin, A. A. Theoretical and Experimental Aspects of the Effects of Point Defects and Disorder on the Vibrations of Crystals. *Solid State Physics*; Seitz, F., Turnbull, D., Eds.; Academic Press, 1966; Vol. *18*, pp 273−420.
(34) Maradudin, A. A. Theoretical and Experimental Aspects of the Effects of Point Defects and Disorder on the Vibrations of Crystals. *Solid State Physics*; Seitz, F., Turnbull, D., Eds.; Academic Press, 1967; Vol. *19*, pp 1−134.
(35) Dresselhaus, M. S.; Dresselhaus, G.; Saito, R. Physics of Carbon Nanotubes. *Carbon* **1995**, *33*, 883−891.
(36) Avouris, P.; Chen, Z.; Perebeinos, V. Carbon-Based Electronics. In *Nanoscience and Technology*; Macmillan Publishers Ltd: U.K., 2009; pp 174−184.
(37) Xiao, Y.; Yan, X. H.; Cao, J. X.; Ding, J. W.; Mao, Y. L.; Xiang, J. Specific Heat and Quantized Thermal Conductance of Single-Walled Boron Nitride Nanotubes. *Phys. Rev. B: Condens. Matter Mater. Phys.* **2004**, *69*, 205415.
(38) Islam, Md. S.; Ushida, K.; Tanaka, S.; Makino, T.; Hashimoto, A. Analysis of Vibrational Properties of C-Doped Hexagonal Boron Nitride (h-BN). *Comput. Mater. Sci.* **2014**, *94*, 225−233.
(39) Islam, M. S.; Anindya, K. N.; Bhuiyan, A. G.; Tanaka, S.; Makino, T.; Hashimoto, A. Effect of 10B Isotope and Vacancy Defects on the Phonon Modes of Two-Dimensional Hexagonal Boron Nitride. *Jpn. J. Appl. Phys.* **2017**, *57*, 02CB04.
(40) Anindya, K. N.; Islam, Md. S.; Hashimoto, A.; Park, J. Combined Effect of 13C Isotope and Vacancies on the Phonon Properties in AB Stacked Bilayer Graphene. *Carbon* **2020**, *168*, 22−31.
(41) Islam, Md. S.; Ushida, K.; Tanaka, S.; Hashimoto, A. Numerical Experiments on Phonon Properties of Isotope and Vacancy-Type Disordered Graphene. *Diamond Relat. Mater.* **2013**, *40*, 115−122.
(42) Tran, V.-T.; Saint-Martin, J.; Dollfus, P.; Volz, S. High Thermoelectric and Electronic Performance in Graphene Nanoribbons by Isotope and Vacancy Engineering. *Mater. Today: Proc.* **2018**, *5*, 10393−10400.
(43) Rodriguez-Nieva, J. F.; Saito, R.; Costa, S. D.; Dresselhaus, M. S. Effect of ^{13}C Isotope Doping on the Optical Phonon Modes in Graphene: Localization and Raman Spectroscopy. *Phys. Rev. B: Condens. Matter Mater. Phys.* **2012**, *85*, 245406.
(44) Miyauchi, Y.; Maruyama, S. Identification of an Excitonic Phonon Sideband by Photoluminescence Spectroscopy of Single-Walled Carbon-13 Nanotubes. *Phys. Rev. B: Condens. Matter Mater. Phys.* **2006**, *74*, 035415.
(45) Sun, C. Q. Lattice Dynamics: Phonon Relaxation. In *Relaxation of the Chemical Bond: Skin Chemisorption Size Matter ZTP Mechanics H2O Myths*; Sun, C. Q., Ed.; Springer: Singapore, 2014; pp 299−312.
(46) Islam, Md. S.; Ushida, K.; Tanaka, S.; Hashimoto, A. Numerical Analysis on Vacancy Induced Vibrational Properties of Graphene Nanoribbons. *Comput. Mater. Sci.* **2013**, *79*, 356−361.

https://doi.org/10.1021/acsomega.2c02792
ACS Omega 2022, 7, 26591−26600

(47) Islam, Md. S.; Ushida, K.; Tanaka, S.; Makino, T.; Hashimoto, A. Effect of Boron and Nitrogen Doping with Native Point Defects on the Vibrational Properties of Graphene. *Comput. Mater. Sci.* **2014**, *94*, 35−43.
(48) Anindya, K. N.; Islam, M. S.; Park, J.; Bhuiyan, A. G.; Hashimoto, A. Interlayer Vacancy Effects on the Phonon Modes in AB Stacked Bilayer Graphene Nanoribbon. *Curr. Appl. Phys.* **2020**, *20*, 572−581.
(49) Haskins, J.; Kınacı, A.; Sevik, C.; Sevinçli, H.; Cuniberti, G.; Çağın, T. Control of Thermal and Electronic Transport in Defect-Engineered Graphene Nanoribbons. *ACS Nano* **2011**, *5*, 3779−3787.
(50) Bi, K.; Chen, Y.; Yang, J.; Wang, Y.; Chen, M. Molecular Dynamics Simulation of Thermal Conductivity of Single-Wall Carbon Nanotubes. *Phys. Lett. A* **2006**, *350*, 150−153.
(51) Feng, D.-L.; Feng, Y.-H.; Chen, Y.; Li, W.; Zhang, X.-X. Effects of Doping, Stone—Wales and Vacancy Defects on Thermal Conductivity of Single-Wall Carbon Nanotubes. *Chin. Phys. B* **2013**, *22*, 016501.
(52) Howlader, A. H.; Islam, M. S. Phonon Transmission of Vacancy Defected (10,0) Carbon Nanotube. *3rd International Conference on Electrical Information and Communication Technology, EICT*; Institute of Electrical and Electronics Engineers, 2017; pp 1−4.
(53) Howlader, A. H.; Islam, Md. S.; Ferdous, N. Phonon Transmission of Vacancy Disordered Armchair Silicene Nanoribbon. *Optoelectron. Lett.* **2021**, *17*, 454−458.
(54) Howlader, A. H.; Islam, M. S.; Islam, A. S. M. J. A Study on Phonon Transmission of (10,0) Silicon Nanotube with Atomic Vacancies. *International Conference of Computer and Information Technology*; Institute of Electrical and Electronics Engineers, 2018; pp 1−4..
(55) Xie, G.; Shen, Y.; Wei, X.; Yang, L.; Xiao, H.; Zhong, J.; Zhang, G. A Bond-Order Theory on the Phonon Scattering by Vacancies in Two-Dimensional Materials. *Sci. Rep.* **2014**, *4*, 5085.
(56) Mingo, N.; Broido, D. A. Length Dependence of Carbon Nanotube Thermal Conductivity and the "Problem of Long Waves. *Nano Lett.* **2005**, *5*, 1221−1225.
(57) Mahan, G. D.; Jeon, G. S. Flexure Modes in Carbon Nanotubes. *Phys. Rev. B: Condens. Matter Mater. Phys.* **2004**, *70*, 075405.
(58) Mariani, E.; von Oppen, F. Temperature-Dependent Resistivity of Suspended Graphene. *Phys. Rev. B: Condens. Matter Mater. Phys.* **2010**, *82*, 195403.
(59) Ochoa, H.; Castro, E. V.; Katsnelson, M. I.; Guinea, F. Scattering by Flexural Phonons in Suspended Graphene under Back Gate Induced Strain. *Phys. E* **2012**, *44*, 963−966.
(60) Simon, F.; Kramberger, Ch.; Pfeiffer, R.; Kuzmany, H.; Zólyomi, V.; Kürti, J.; Singer, P. M.; Alloul, H. Isotope Engineering of Carbon Nanotube Systems. *Phys. Rev. Lett.* **2005**, *95*, 017401.
(61) Harman, T. C.; Taylor, P. J.; Walsh, M. P.; LaForge, B. E. Quantum Dot Superlattice Thermoelectric Materials and Devices. *Science* **2002**, *297*, 2229−2232.
(62) Hochbaum, A. I.; Chen, R.; Delgado, R. D.; Liang, W.; Garnett, E. C.; Najarian, M.; Majumdar, A.; Yang, P. Enhanced Thermoelectric Performance of Rough Silicon Nanowires. *Nature* **2008**, *451*, 163−167.
(63) Boukai, A. I.; Bunimovich, Y.; Tahir-Kheli, J.; Yu, J.-K.; Goddard III, W. A., III; Heath, J. R. Silicon Nanowires as Efficient Thermoelectric Materials. *Nature* **2008**, *451*, 168−171.
(64) Li, X.; Chen, J.; Yu, C.; Zhang, G. Comparison of Isotope Effects on Thermal Conductivity of Graphene Nanoribbons and Carbon Nanotubes. *Appl. Phys. Lett.* **2013**, *103*, 013111.
(65) Landry, E. S.; McGaughey, A. J. H. Thermal Boundary Resistance Predictions from Molecular Dynamics Simulations and Theoretical Calculations. *Phys. Rev. B: Condens. Matter Mater. Phys.* **2009**, *80*, 165304.
(66) Che, J.; Çagin, T.; Goddard, W. A. Thermal Conductivity of Carbon Nanotubes. *Nanotechnology* **2000**, *11*, 65−69.
(67) Kramer, B.; MacKinnon, A. Localization: Theory and Experiment. *Rep. Prog. Phys.* **1993**, *56*, 1469−1564.
(68) Javey, A.; Guo, J.; Wang, Q.; Lundstrom, M.; Dai, H. Ballistic Carbon Nanotube Field-Effect Transistors. *Nature* **2003**, *424*, 654−657.

https://doi.org/10.1021/acsomega.2c02792
ACS Omega 2022, 7, 26591−26600